Electronic Supplementary Material (ESI) for Physical Chemistry Chemical Physics.

Supplementary information

DFT Benchmark Studies on Representative Species and Poisons of Methane Steam Reforming on Ni(111)

Sai Sharath Yadavalli[1], Glenn Jones[2] and Michail Stamatakis[1*]

[1] Thomas Young Centre and Department of Chemical Engineering, University College London, Roberts Building, Torrington Place, London WC1E 7JE, United Kingdom

[2] Johnson Matthey Technology Centre, Sonning Common, Reading RG4 9NH, United Kingdom

[*] e-mail: m.stamatakis@ucl.ac.uk

Table S1. The lattice constant predictions of DFT functionals

Functional	Ni Lattice constant prediction (Å)	Graphene Lattice constant prediction (Å)
PBE	3.522	-
RPBE	3.557	-
revPBE	3.547	-
PBE-D3	3.481	2.467
RPBE-D3	3.487	2.479
revPBE-D3	3.467	2.476
PBE-dDsC	3.502	2.467
PBE-TS	3.419	2.465
optB86b-vdW	3.493	2.466
optB88-vdW	3.514	2.465
optPBE-vdW	3.533	2.471
BEEF-vdW	3.540	2.466

Note: The experimental lattice constant value of Ni is 3.524 Å.[1] The experimental graphene-Ni lattice constant value is 2.464 Å.[2] The pure graphene DFT calculations have been carried out using a 5×5×1 k-point grid. For the PBE, RPBE and revPBE functionals we did not calculate the pure graphene configurations, since graphene does not bind on Ni using these functionals.

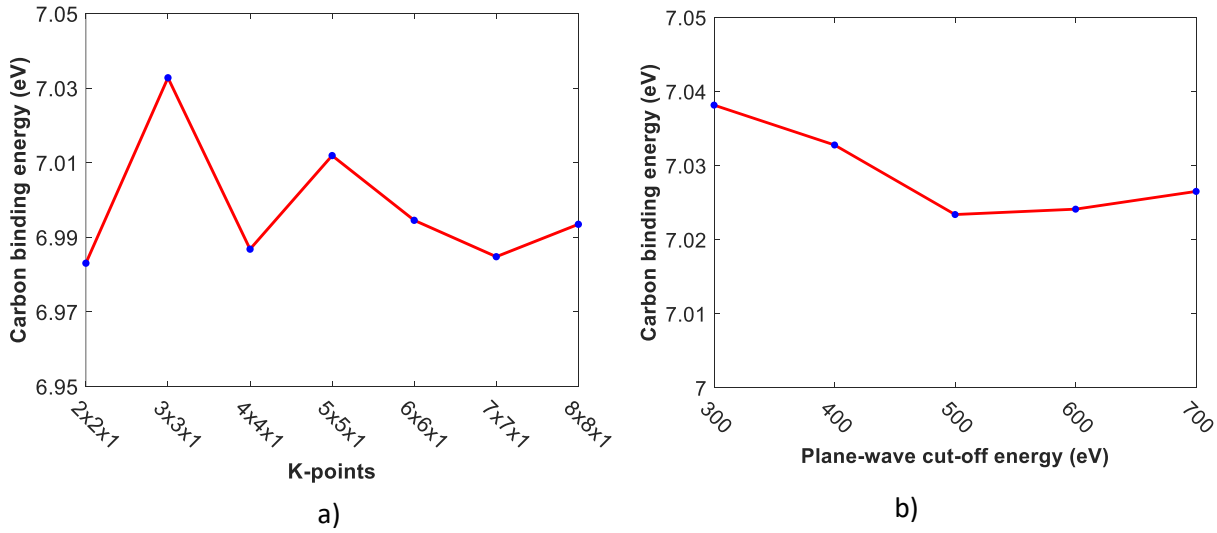

Figure S1: The convergence plots of carbon binding energy on Ni(111) using the PBE-D3 functional: (a) K-points convergence test and (b) Plane-wave cut-off energy convergence study.

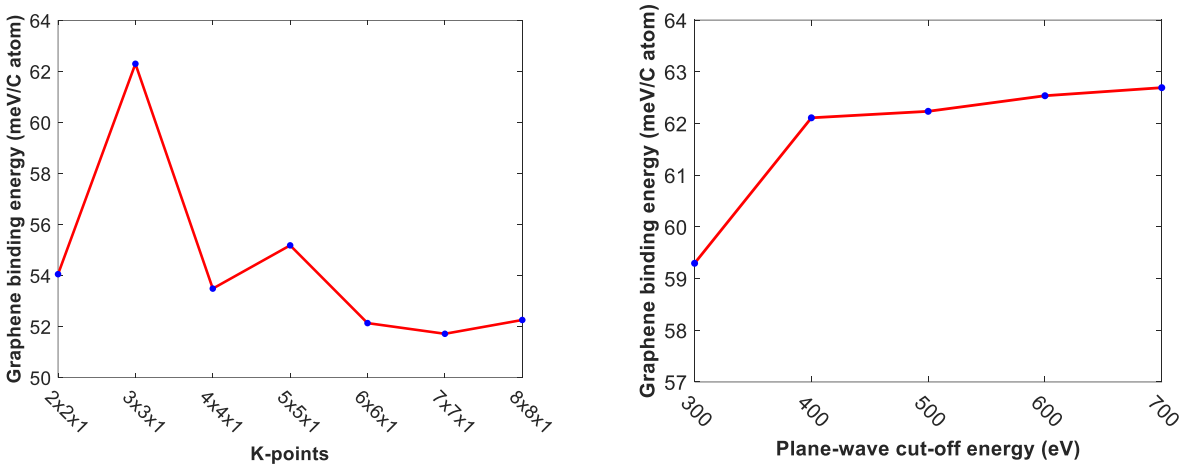

a) b)

Figure S2: The convergence plots of graphene binding energy on Ni(111) using the PBE-D3 functional: (a) K-points convergence test and (b) Plane-wave cut-off energy convergence study.

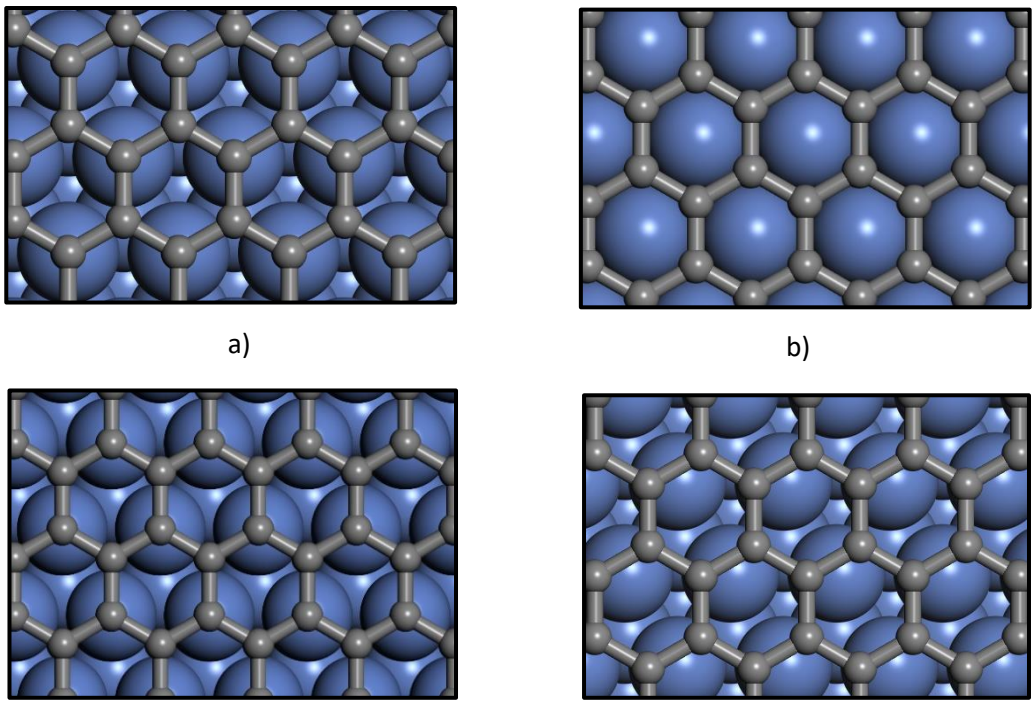

a) b)

c) d)

Figure S3: Graphene configurations include a) top-hcp configuration, b) fcc-hcp configuration, c) top-fcc configuration and d) bridge-top configuration.[3] The schematics have the following convention: The atoms in blue represent Ni and the atoms in grey are carbon.

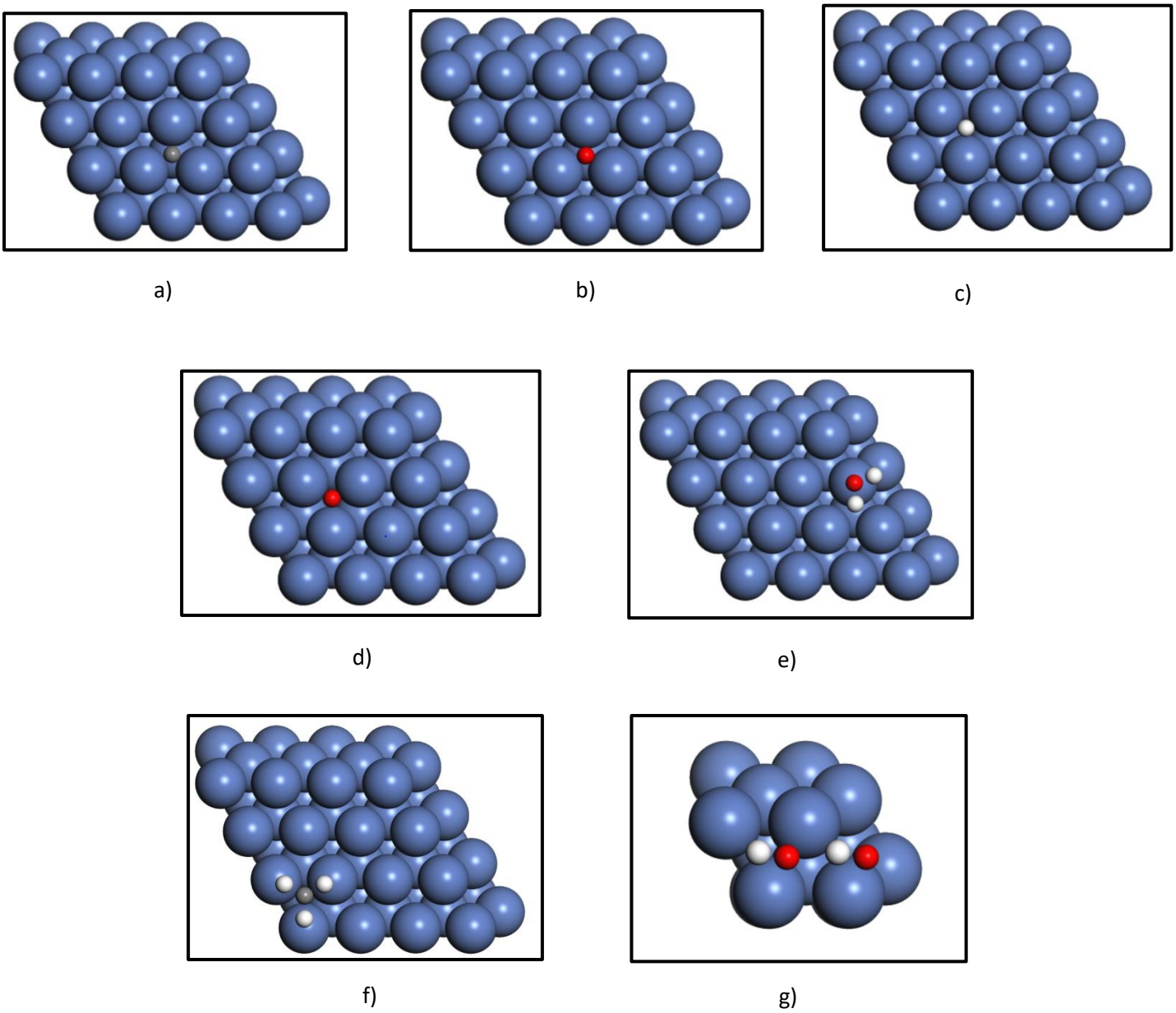

Figure S4: The preferred binding sites of MSR intermediates: a) The carbon atom occupies the hcp site. b) The CO molecule binds on the hcp site. c) The hydrogen atom is stable on the fcc site. d) The oxygen atom occupies the fcc site. e) The H_2O molecule physisorbs on the top site. f) The CH_3 molecule binds on the fcc site. g) The two OH atoms are stable on the three-fold hollow sites. The schematics have the following convention: The atoms in blue represent Ni, the atoms in grey are carbon, the atoms in red indicate oxygen and the atoms in white are hydrogen.

Table S2. Evaluating the performance of DFT functionals in predicting the energies of gas-phase reactions relevant to MSR, as well as graphite formation

Method/Functional	$E_{rxn-gasph}^{MSR}$ (eV)	$E_{rxn-gasph}^{H2O\ diss}$ (eV)	$E_{coh}^{graphite}$ (eV)	$E_{bind}^{graphite}$ (meV/C)
CCSD(T) or experiment	2.82[4,5]	5.48[4,5]	7.37[6]	48[6]
PBE	3.18	5.07	7.97	-14.04
RPBE	2.80	4.78	7.53	-36.68
revPBE	2.83	4.81	7.58	-35.75
PBE-D3	3.18	5.07	8.07	46.69
RPBE-D3	2.83	4.78	7.69	48.43
revPBE-D3	2.85	4.81	7.75	62.09
PBE-dDsC	3.18	5.07	8.22	63.03
PBE-TS	3.18	5.07	8.11	82.34
optB86b-vdW	2.81	4.92	8.07	69.91
optB88-vdW	2.68	4.89	7.98	69.56
optPBE-vdW	2.59	4.79	7.84	63.21
BEEF-vdW	2.51 (±0.26)	4.70 (±0.17)	7.64 (±0.23)	36.68 (±19.24)

Notes: $E_{rxn-gasph}^{MSR}$ indicates the MSR reaction energy – $CH_4(g) + H_2O(g) \rightleftarrows CO(g) + 3H_2(g)$, $E_{rxn-gasph}^{H2O\ diss}$ represents the reaction energy of H_2O dissociation – $2H_2O(g) \rightleftarrows 2H_2(g) + O_2(g)$, $E_{coh}^{graphite}$ and $E_{bind}^{graphite}$ are the graphite cohesive energy and graphite interlayer binding energy, respectively. $E_{rxn-gasph}^{MSR}$ and $E_{rxn-gasph}^{H2O\ diss}$ are derived from a CCSD(T) atomisation energies dataset which does not include ZPE/thermal corrections. $E_{coh}^{graphite}$ and $E_{bind}^{graphite}$ are obtained from experimental works reported in the literature. The graphite bulk calculations (with a supercell that contains four carbon atoms) have been performed using a k-point mesh of size 21×21×7 and a plane-wave cut-off energy value of 400 eV (refer to Figures S5(a) and S5(b) for convergence plots). The lattice vectors of graphite bulk are obtained from experimental data available in the literature.[6]

Interestingly, all the DFT functionals have varying performance for each of the gas-phase systems. According to Table S2, the RPBE, revPBE, RPBE-D3, revPBE-D3 and optB86b-vdW functionals predict the MSR reaction energy with high accuracy. The PBE functional and its corresponding dispersion-corrected flavours (PBE-D3, PBE-dDsC and PBE-TS) overestimate the MSR reaction energy by 0.36 eV. Whereas the vdW-DF such as optB88-vdW, optPBE-vdW and BEEF-vdW substantially underpredict the MSR reaction energy (refer to Table S2).

Most of the DFT functionals exhibit large deviations in predicting the reaction energy of H_2O dissociation (as shown in Table S2). Wellendorff *et al.*[4] have also reported that the DFT functionals do not give a good description of H_2O dissociation in the gas phase. The inability of DFT functionals to provide an accurate estimate of the triplet O_2(g) energy is considered to be the primary reason for such a poor performance.[4] The RPBE and revPBE functionals predict the graphite cohesive energy with reasonable accuracy. Other DFT functionals tend to significantly overpredict the cohesive energy of graphite (refer to Table S2). The benchmark study conducted by Rêgo *et al.*[6] also concludes that the dispersion-inclusive DFT functionals overestimate graphite cohesive energy. The GGA functionals fail to capture the van der Waals interactions between consecutive layers of graphite. As shown in Table S2, these functionals predict a negative value (repulsive interaction) for the interlayer binding energy of graphite. Among the DFT-D functionals, the PBE-D3 and RPBE-D3 functionals accurately reproduce the graphite interlayer interactions. The predictions of PBE-dDsC and revPBE-D3 functionals are also in reasonable agreement with the experimental result. In contrast, the PBE-TS functional substantially overpredicts the interlayer binding energy of graphite. The vDW-DF predict the graphite interlayer interactions with acceptable accuracy (refer to Table S2).

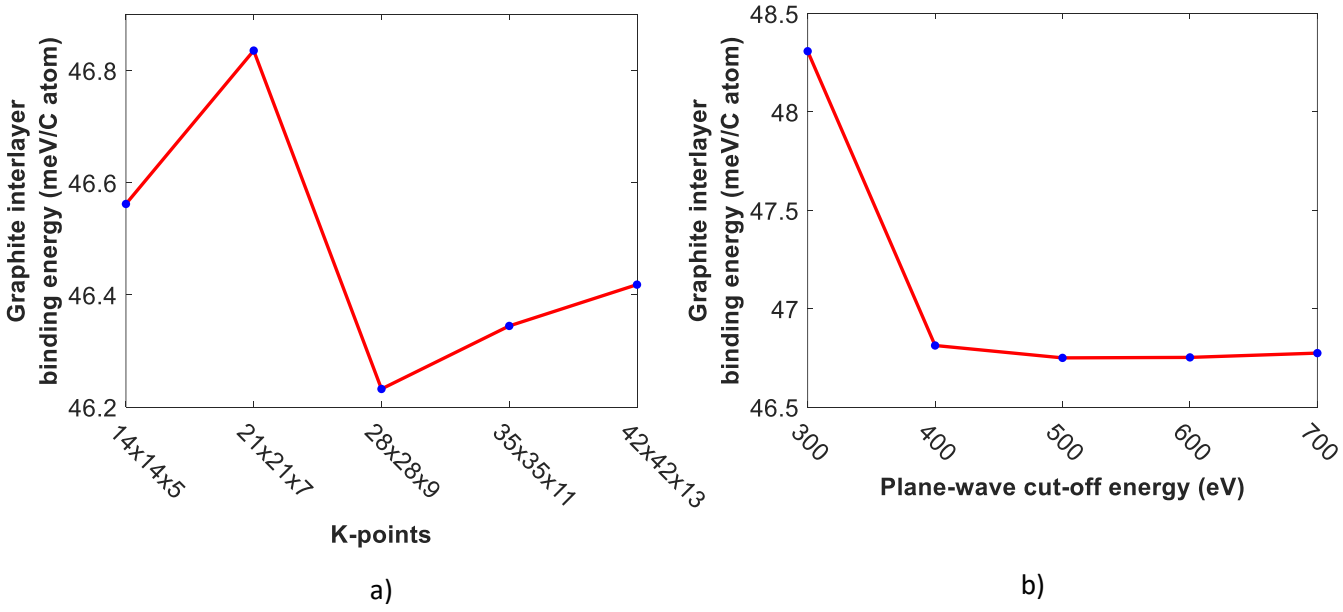

Figure S5: The convergence plots of graphite bulk system using the PBE-D3 functional: (a) K-points convergence test and (b) Plane-wave cut-off energy convergence study.

Table S3. Comparison of DFT predictions of oxygen binding energy predictions obtained using two different approaches

Functional	$E_{O\ bind}^{method1}$ (eV)	$E_{O\ bind}^{method2}$ (eV)	Deviation of $E_{method1}^{O\ bind}$ from the experimental value (eV)	Deviation of $E_{method2}^{O\ bind}$ from the experimental value (eV)
PBE	5.09	4.68	0.56	0.14
RPBE	4.84	4.13	0.30	-0.41
revPBE	4.87	4.20	0.34	-0.34
PBE-D3	5.17	4.75	0.63	0.22
RPBE-D3	4.97	4.27	0.44	-0.27
revPBE-D3	5.02	4.34	0.48	-0.19
PBE-dDsC	5.20	4.79	0.67	0.25
PBE-TS	5.04	4.63	0.51	0.09
optB86b-vdW	5.81	5.25	1.28	0.71
optB88-vdW	5.88	5.28	1.34	0.75
optPBE-vdW	5.76	5.06	1.23	0.53
BEEF-vdW	5.23	4.44	0.69	-0.09
Experimental value	4.53 (±0.2)		-	

Note: Two methods are used to determine the O_2(g) energy: 1) The O_2(g) energy is estimated by using the following equation: $E_{O2gasph}^{method1} = E_{rxn-gasph}^{H2O\ diss} + 2E_{gasph}^{H2O} - 2E_{gasph}^{H2}$. The terms $E_{rxn-gasph}^{H2O\ diss}$, E_{gasph}^{H2O} and E_{gasph}^{H2} refer to the gas-phase reaction energy of H_2O dissociation (the value is 5.48 eV; it is derived from a CCSD(T) atomisation energies dataset),[5] H_2O gas-phase energy and H_2 gas-phase energy (both these energies are computed using DFT), respectively. The O_2(g) energy obtained from method 1 ($E_{O2gasph}^{method1}$) is used to estimate the term $E_{O\ bind}^{method1}$ 2) The O_2 gas-phase energy is computed by performing a DFT calculation (the corresponding oxygen binding energy obtained under this approach is labelled as $E_{O\ bind}^{method2}$)

As discussed previously, the DFT functionals give an inaccurate value of the energy of O_2 gas-phase triplet state. In an effort to correct this error, we estimated the O_2 gas-phase energy from the reaction energy of H_2O dissociation (please refer to the "Note" given below Table S3 for more details). As shown in Table S3, the oxygen binding energies ($E_{O\ bind}^{method1}$) obtained using this approach deviate significantly from the experimental data (refer to the third column of Table S3). In a recent study, Wellendorff *et al.*[4] have made similar observations for a few systems. A plausible explanation for this behaviour could be that the total energy of the bound state - O/Ni(111) - is also estimated poorly by the DFT functionals, and thus, the binding energy predictions of oxygen obtained using an accurate O_2 gas-phase energy exhibit large deviations. On the other hand, the oxygen binding energies estimated by using the DFT predicted O_2(g) energy ($E_{O\ bind}^{method2}$) have a better agreement with the experimental value (refer

to the last column of Table S3). In this case, it is possible that there is a cancellation of error between the DFT energies of the bound state and the gas-phase. Hence, the DFT results of the second approach ($E_{O\ bind}^{method2}$) are presented in Table 3 of the "Results and Discussion" section.

Table S4. The predictions of DFT functionals for MSR species (without ZPE and thermal corrections)

DFT predictions without ZPE and thermal corrections (eV)									
Functional	CO	H_2O	2×H	2×O	OH	C	CH_3	CH_4-diss	C-oxid
PBE	1.93	0.30	1.12	4.72	3.27	6.93	1.95	0.05	1.69
RPBE	1.54	0.10	0.79	4.17	2.90	6.46	1.51	-0.43	1.94
revPBE	1.60	0.10	0.83	4.24	2.94	6.53	1.56	-0.37	1.90
PBE-D3	2.12	0.53	1.33	4.80	3.41	7.01	2.32	0.53	1.61
RPBE-D3	1.84	0.46	1.07	4.31	3.14	6.62	2.06	0.25	1.78
revPBE-D3	1.92	0.52	1.17	4.39	3.18	6.69	2.22	0.45	1.73
PBE-dDsC	2.09	0.46	1.22	4.83	3.64	7.05	2.19	0.34	1.58
PBE-TS	2.26	0.64	1.30	4.67	3.57	7.03	2.45	0.64	1.59
optB86b-vdW	2.17	0.53	1.15	5.29	3.53	7.08	2.37	0.45	1.57
optB88-vdW	2.01	0.50	1.02	5.33	3.49	6.94	2.18	0.23	1.74
optPBE-vdW	1.88	0.45	0.92	5.11	3.37	6.79	2.05	0.08	1.82
BEEF-vdW	1.61	0.28	0.68	4.48	3.10	6.44	1.70	-0.28	2.05

Note: The computational errors of BEEF-vdW functional are not reported in Table S4.

Table S5. The ZPE corrections recorded for each of the DFT functionals

ZPE corrections (eV)								
Functional	CO	H2O	2×H	2×O	OH	C	CH3	CH_4-diss
PBE	-0.05	-0.06	-0.09	-0.06	-0.15	-0.10	-0.10	0.12
RPBE	-0.05	-0.06	-0.07	-0.06	-0.15	-0.10	-0.10	0.12
revPBE	-0.05	-0.06	-0.08	-0.06	-0.15	-0.10	-0.10	0.12
PBE-D3	-0.05	-0.06	-0.09	-0.06	-0.14	-0.10	-0.10	0.12
RPBE-D3	-0.05	-0.07	-0.07	-0.06	-0.15	-0.10	-0.09	0.13
revPBE-D3	-0.05	-0.07	-0.08	-0.06	-0.14	-0.10	-0.10	0.12
PBE-dDsC	-0.05	-0.06	-0.09	-0.06	-0.15	-0.10	-0.10	0.12
PBE-TS	-0.05	-0.06	-0.09	-0.06	-0.14	-0.10	-0.10	0.11
optB86b-vdW	-0.05	-0.07	-0.08	-0.07	-0.15	-0.10	-0.09	0.13
optB88-vdW	-0.05	-0.07	-0.08	-0.07	-0.15	-0.10	-0.09	0.13
optPBE-vdW	-0.05	-0.07	-0.07	-0.06	-0.15	-0.10	-0.10	0.13
BEEF-vdW	-0.05	-0.06	-0.07	-0.06	-0.15	-0.10	-0.10	0.12

Note: The ZPE corrections are not included for the carbon dissociation reaction (refer to Table 2 under the subsection "DFT benchmarks of MSR species" for more details).

Table S6. The thermal corrections recorded for each of the DFT functionals

Thermal corrections (eV)							
Functional	CO	H2O	2×O	OH	C	CH_3	CH_4-diss
PBE	-0.006	0.010	0.017	0.026	0.003	0.028	0.027
RPBE	-0.007	0.009	0.014	0.025	0.001	0.026	0.026
revPBE	-0.007	0.008	0.015	0.025	0.002	0.027	0.026
PBE-D3	-0.006	0.010	0.017	0.025	0.003	0.029	0.028
RPBE-D3	-0.007	0.009	0.014	0.025	0.002	0.025	0.025
revPBE-D3	-0.007	0.010	0.015	0.025	0.002	0.027	0.026
PBE-dDsC	-0.005	0.009	0.017	0.026	0.003	0.029	0.028
PBE-TS	-0.005	0.007	0.017	0.025	0.004	0.029	0.028
optB86b-vdW	-0.006	0.011	0.019	0.026	0.003	0.028	0.028
optB88-vdW	-0.006	0.011	0.019	0.026	0.003	0.027	0.027
optPBE-vdW	-0.007	0.010	0.017	0.025	0.002	0.026	0.026
BEEF-vdW	-0.008	0.009	0.015	0.025	0.001	0.026	0.025

Note: The thermal corrections are not included for the hydrogen adsorption and carbon oxidation reactions (refer to Table 2 under the subsection “DFT benchmarks of MSR species” for more details).

Table S7. The estimated vibrational wavenumbers of hydroxyl

Functional	Bound state wave numbers (cm^{-1})												gas phase wave numbers (cm^{-1})
PBE	3247	3171	1056	940	792	776	538	428	340	254	220	136	3603
RPBE	3325	3261	1028	913	763	756	520	413	322	241	206	135	3596
revPBE	3304	3237	1038	922	772	760	524	415	324	243	209	135	3595
PBE-D3	3197	3105	1074	958	800	776	564	429	338	249	210	135	3603
RPBE-D3	3268	3185	1088	973	792	764	563	421	324	237	190	138	3595
revPBE-D3	3225	3129	1078	968	791	765	576	423	323	237	188	132	3598
PBE-dDsC	3187	3075	1068	938	824	772	602	425	339	250	211	137	3532
PBE-TS	3126	3013	1104	983	814	776	606	436	337	248	199	137	3603
optB86b-vdW	3213	3133	1061	941	789	775	561	437	344	262	223	138	3579
optB88-vdW	3273	3205	1053	929	785	778	553	437	349	260	222	139	3585
optPBE-vdW	3309	3247	1033	911	767	765	542	422	334	253	214	135	3574
BEEF-vdW	3440	3390	1023	898	762	756	540	420	332	251	207	132	3643

Note: The bound state wave numbers (mentioned above) have been calculated for two OH species adsorbed on Ni(111).

Table S8. The estimated vibrational wavenumbers of carbon monoxide

Functional	Bound state wave numbers (cm^{-1})						gas phase wave numbers (cm^{-1})
PBE	1763	344	283	282	143	143	2126
RPBE	1740	332	273	273	138	137	2103
revPBE	1745	335	277	276	141	141	2108
PBE-D3	1770	350	283	283	143	143	2126
RPBE-D3	1749	342	277	277	138	137	2103
revPBE-D3	1756	344	278	278	137	137	2108
PBE-dDsC	1766	350	284	284	145	144	2126
PBE-TS	1778	359	291	291	144	144	2126
optB86b-vdW	1762	347	283	283	143	143	2125
optB88-vdW	1757	337	279	279	142	142	2131
optPBE-vdW	1744	336	272	271	138	137	2116
BEEF-vdW	1757	333	271	271	138	138	2124

Table S9. The estimated vibrational wavenumbers of oxygen

Functional	Bound state wave numbers (cm^{-1})			gas phase wave numbers (cm^{-1})
PBE	488	393	393	1566
RPBE	470	374	373	1544
revPBE	473	378	377	1549
PBE-D3	498	389	389	1566
RPBE-D3	485	372	372	1544
revPBE-D3	495	376	376	1549
PBE-dDsC	490	393	393	1566
PBE-TS	516	381	381	1566
optB86b-vdW	502	404	404	1554
optB88-vdW	498	406	406	1535
optPBE-vdW	483	394	394	1526
BEEF-vdW	472	378	378	1551

Table S10. The estimated vibrational wavenumbers of hydrogen

Functional	Bound state wave numbers (cm^{-1})			gas phase wave numbers (cm^{-1})
PBE	1133	861	860	4307
RPBE	1103	831	830	4340
revPBE	1112	838	838	4334
PBE-D3	1150	857	857	4307
RPBE-D3	1114	810	810	4340
revPBE-D3	1136	847	846	4334
PBE-dDsC	1146	864	864	4307
PBE-TS	1198	841	840	4307
optB86b-vdW	1137	849	849	4301
optB88-vdW	1112	854	853	4349
optPBE-vdW	1101	834	834	4349
BEEF-vdW	1108	836	836	4447

Table S11. The estimated vibrational wavenumbers of carbon

Functional	Bound state wave numbers (cm^{-1})		
PBE	561	549	549
RPBE	545	534	533
revPBE	549	537	537
PBE-D3	579	540	540
RPBE-D3	574	525	525
PBE-dDsC	568	549	549
PBE-TS	612	530	530
revPBE-D3	583	525	525
optB86b-vdW	572	547	547
optB88-vdW	558	548	547
optPBE-vdW	551	539	539
BEEF-vdW	545	526	526

Table S12. The estimated vibrational wavenumbers of water

Functional	Bound state wave numbers (cm^{-1})									gas phase wave numbers (cm^{-1})		
PBE	3686	3578	1543	463	449	203	94	82	49	3831	3716	1584
RPBE	3720	3610	1569	423	413	147	87	77	58	3820	3705	1596
revPBE	3719	3608	1565	429	418	150	86	80	51	3823	3708	1594
PBE-D3	3658	3552	1536	482	480	212	107	93	27	3831	3716	1584
RPBE-D3	3645	3542	1551	519	498	187	121	90	15	3820	3703	1595
revPBE-D3	3655	3549	1550	530	515	184	139	103	25	3823	3707	1593
PBE-dDsC	3673	3566	1538	471	460	215	93	84	34	3831	3716	1584
PBE-TS	3673	3565	1538	445	440	193	86	79	15	3831	3716	1584
optB86b-vdW	3639	3530	1538	495	466	229	101	87	66	3807	3692	1584
optB88-vdW	3654	3545	1550	493	461	235	94	86	57	3807	3694	1596
optPBE-vdW	3662	3553	1559	478	446	201	91	80	58	3797	3684	1597
BEEF-vdW	3772	3661	1597	452	420	156	86	78	63	3875	3761	1624

Table S13. The estimated vibrational wavenumbers of methane

Functional	gas phase wave numbers (cm^{-1})								
PBE	3092	3091	3091	2975	1512	1511	1286	1286	1285
RPBE	3085	3085	3083	2969	1517	1516	1294	1294	1294
revPBE	3087	3087	3085	2971	1517	1516	1293	1293	1293
PBE-D3	3092	3091	3090	2974	1511	1510	1286	1286	1285
RPBE-D3	3071	3070	3069	2951	1512	1511	1293	1293	1292
revPBE-D3	3079	3079	3077	2960	1513	1512	1292	1291	1291
PBE-dDsC	3092	3092	3091	2976	1512	1511	1287	1287	1286
PBE-TS	3092	3091	3091	2975	1511	1511	1286	1286	1285
optB86b-vdW	3067	3066	3065	2959	1516	1515	1294	1294	1293
optB88-vdW	3072	3068	3067	2971	1535	1529	1316	1313	1310
optPBE-vdW	3063	3062	3061	2965	1529	1528	1311	1310	1310
BEEF-vdW	3104	3103	3101	2999	1550	1549	1330	1330	1329

Table S14. The estimated vibrational wavenumbers of methyl (bound state)

Functional	Bound state wave numbers (cm^{-1})											
PBE	2826	2824	2764	1292	1291	1170	479	478	402	350	219	218
RPBE	2862	2861	2799	1318	1318	1170	490	488	378	323	193	191
revPBE	2856	2855	2792	1313	1313	1169	485	484	383	329	198	197
PBE-D3	2832	2831	2766	1286	1286	1166	479	479	399	360	224	224
RPBE-D3	2862	2862	2792	1299	1299	1151	456	455	342	334	190	189
revPBE-D3	2857	2857	2785	1291	1291	1149	463	463	371	354	209	209
PBE-dDsC	2824	2822	2761	1289	1288	1172	476	475	408	357	226	225
PBE-TS	2846	2845	2783	1298	1298	1174	495	494	399	362	223	222
optB86b-vdW	2778	2777	2724	1290	1290	1176	471	471	398	354	222	222
optB88-vdW	2810	2809	2760	1318	1318	1185	474	473	387	343	208	208
optPBE-vdW	2824	2823	2773	1326	1326	1182	481	481	375	328	195	194
BEEF-vdW	2895	2893	2836	1359	1359	1195	502	501	369	327	189	187

Table S15. The estimated vibrational wavenumbers of methyl (gas phase)

Functional	gas phase wave numbers (cm^{-1})					
PBE	3234	3232	3054	1356	1356	524
RPBE	3226	3226	3047	1363	1363	509
revPBE	3227	3227	3048	1362	1362	513
PBE-D3	3232	3231	3052	1356	1355	525
RPBE-D3	3217	3216	3036	1363	1362	516
revPBE-D3	3220	3220	3038	1360	1360	518
PBE-dDsC	3234	3233	3055	1357	1357	525
PBE-TS	3234	3233	3054	1356	1356	525
optB86b-vdW	3212	3211	3036	1362	1361	519
optB88-vdW	3223	3221	3049	1375	1373	529
optPBE-vdW	3215	3215	3043	1376	1376	521
BEEF-vdW	3258	3258	3082	1396	1396	531

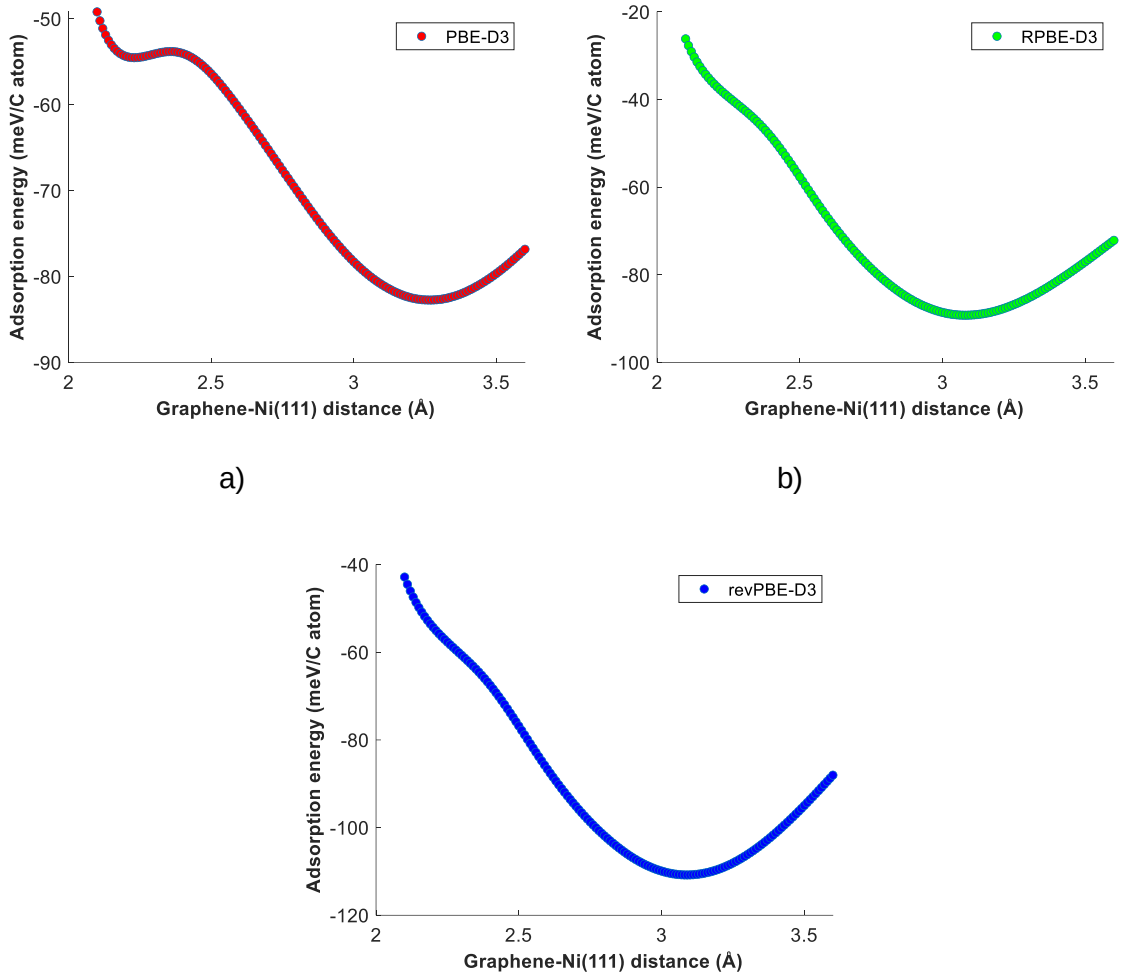

Figure S6: The potential energy profiles of graphene-Ni(111) (top-fcc geometry) using DFT-D3 functionals – (a) PBE-D3, (b) RPBE-D3 and (c) revPBE-D3 (up to the global minimum).

Table S16. The geometric details of two distinct graphene-Ni(111) simulation setups used for the PBE-TS functional.

Graphene-Ni(111) configuration	Ni lattice constant (Å)	Graphene lattice constant (bound on Ni(111)) (Å)	Deviation (%) from experimental Ni lattice constant (Å)	Deviation (%) from experimental graphene lattice constant (Å)
System 1	3.419	2.418	-2.97	-1.87
System 2	3.481	2.461	-1.22	-0.12

Note: The experimental lattice constants of Ni and graphene are 3.524 Å[1] and 2.464 Å[2], respectively.

As shown in Table S16, we carried out DFT calculations for the PBE-TS functional using two disparate graphene-Ni(111) setups. In “System 1”, the PBE-TS optimised Ni lattice constant was used to construct the graphene-Ni(111) supercell. It can be inferred from Table S16 that the Ni lattice constant and the corresponding graphene lattice constant (bound on Ni(111)) of “System 1” are significantly lower than the experimental data. Using “System1”, we do not converge to the shallow first minimum of graphene-Ni(111) primarily because the carbon atoms experience substantial “strain” effects. The optimised graphene-Ni(111) distance of “System 1” is depicted in Figure S7(a). The PBE-D3 optimised Ni lattice constant (which is closer to the experimental value) was used in “System 2” – in this case, the carbon atoms of graphene-Ni(111) experience relatively weaker repulsive interactions. Thus, the PBE-TS calculation of “System 2” converges to the first minimum of graphene-Ni(111) (as shown in Figure S7(b)).

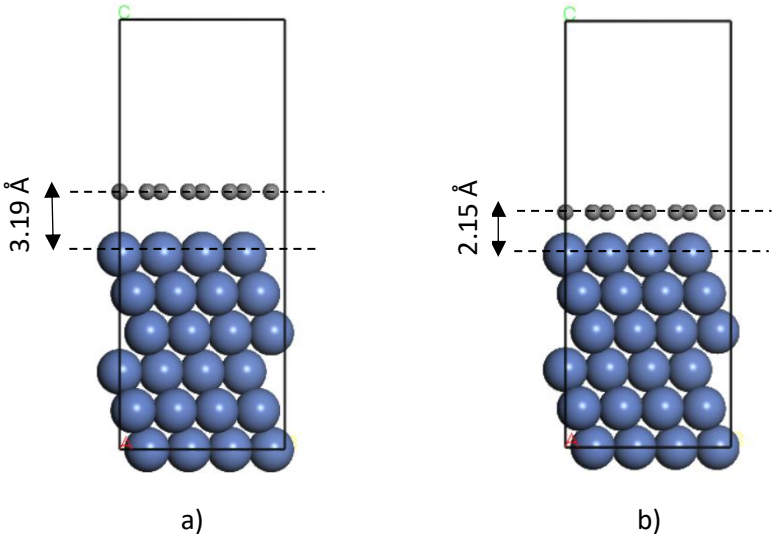

Figure S7: The graphene-Ni(111) optimised configurations obtained using the PBE-TS functional: (a) “System 1” and (b) “System 2”.

References

1. F. Göltl, E. A. Murray, S. A. Tacey, S. Rangarajan and M. Mavrikakis, *Surface Science*, 2020, **700**, 121675.
2. P. Janthon, F. Vines, S. M. Kozlov, J. Limtrakul and F. Illas, *J Chem Phys*, 2013, **138**, 244701.
3. W. Zhao, S. M. Kozlov, O. Höfert, K. Gotterbarm, M. P. A. Lorenz, F. Vines, C. Papp, A. Görling and H.-P. Steinrück, *The Journal of Physical Chemistry Letters*, 2011, **2**, 759-764.
4. J. Wellendorff, T. L. Silbaugh, D. Garcia-Pintos, J. K. Nørskov, T. Bligaard, F. Studt and C. T. Campbell, *Surface Science*, 2015, **640**, 36-44.
5. R. Haunschild and W. Klopper, *Journal of Chemical Physics*, 2012, **136**.
6. C. R. Rego, L. N. Oliveira, P. Tereshchuk and J. L. Da Silva, *J Phys Condens Matter*, 2015, **27**, 415502.